

Bose-Einstein condensation of paraxial light

J. Klaers, J. Schmitt, T. Damm, F. Vewinger and M. Weitz
Institut für Angewandte Physik, Universität Bonn,
Wegelerstr. 8, 53115 Bonn, Germany.
Tel.: +49-228-734836
Fax: +49-228-734835

(Dated: October 7, 2018)

Photons, due to the virtually vanishing photon-photon interaction, constitute to very good approximation an ideal Bose gas, but owing to the vanishing chemical potential a (free) photon gas does not show Bose-Einstein condensation. However, this is not necessarily true for a lower-dimensional photon gas. By means of a fluorescence induced thermalization process in an optical microcavity one can achieve a thermal photon gas with freely adjustable chemical potential. Experimentally, we have observed thermalization and subsequently Bose-Einstein condensation of the photon gas at room temperature. In this paper, we give a detailed description of the experiment, which is based on a dye-filled optical microcavity, acting as a white-wall box for photons. Thermalization is achieved in a photon number-conserving way by photon scattering off the dye molecules, and the cavity mirrors both provide an effective photon mass and a confining potential - key prerequisites for the Bose-Einstein condensation of photons. The experimental results are in good agreement with both a statistical and a simple rate equation model, describing the properties of the thermalized photon gas.

Contents

I. Introduction	1
II. Experimental scheme	2
A. Cavity photon dispersion	3
B. Statistical theory of the photon gas	4
C. Rate equation model	4
III. Experimental setup	6
IV. Thermalization of the transversal photon state	7
A. Spectral and spatial photon distribution	7
B. Redistribution of photons	9
V. Bose-Einstein condensation	10
A. Spectral and spatial photon distribution	10
B. Scaling of the critical power with the resonator geometry	12
C. Condensation by spatial relaxation	12
D. Reabsorption cycles	13
E. Selfinteraction of the light condensate	14
VI. Conclusions	15
Acknowledgments	16
<hr/>	16
References	16

I. INTRODUCTION

Photons have played a vital role for the experimental realization of Bose-Einstein condensation (BEC) [1] in ultracold atomic gases [2–7]. To cool down matter to sufficiently low temperatures, fundamentally new cooling and trapping techniques based on the interaction with light had to be developed. These experimental techniques were rendered possible only by the invention of the laser and even between the birth of the laser and the experimental realization of Bose-Einstein condensation in atomic gases more than thirty years elapsed.

Considering their bosonic nature it seems natural to ask if photons can undergo a BEC in their own right. It is known that a similar phenomenon occurs, when a mode in a laser resonator is macroscopically occupied above the lasing threshold. The oscillation build-up of a laser mode is however not a thermodynamic phase transition in a conventional sense. Neither the state of the light field is in thermal equilibrium nor the lasing threshold can be determined by thermodynamic considerations. To some extent a laser is even a prime example for a system in non-equilibrium: Typically laser gain in a medium is only achieved if the transition at the lasing wavelength is inverted, which can only be achieved under non-equilibrium conditions using external pumping [8–10]. The question, whether a BEC of photons in a strict sense is possible, typically is negated with reference to black body radiation [11, 12] - presumably the most omnipresent Bose gas at all [13, 14]. For black body radiation not only the spectral distribution of the photon energies depends on temperature, but also their total number. Temperature and photon number cannot be tuned independently. If the temperature of the photon gas is lowered then also the photon number will decrease

according to the Stefan-Boltzmann law, preventing the onset of Bose-Einstein condensation.

The last years have seen increasing effort in investigating equilibrium processes that lead to macroscopically occupied photonic states. It is clear that such processes have to conserve the photon number. Presumably the first process to be considered was Compton scattering of x-ray photons in plasmas [15]. Later theoretical work considered the use of cavities for photon condensation, but did not give a route for reaching the thermalization [16]. In an interesting work, photon-photon scattering in a nonlinear medium was investigated [17–26]. Here photons are expected to thermalize due to four-wave mixing which can be interpreted as collisions between two photons - quite similar to binary collisions of atoms. However, this ansatz could not be verified experimentally. The photon-photon interactions in the experimental systems investigated up to now seem to be too weak to achieve a thermalization [19]. In other work, condensation of classical waves in nonlinear or disordered media has been investigated, though the systems are non-thermodynamic [27–30]. Experiments on exciton polariton condensation [31–36] can also be put into the broader context of light condensation. These systems are characterized by a strong coupling of photonic and excitonic degrees of freedom which leads to new energy eigenstates, the exciton polaritons. Due to their excitonic part, which is coherently coupled to the photonic part, the polaritons perform binary collisions, which can lead to a thermalization of the polariton gas.

Recently we have observed a photon number conserving thermalization process of a two-dimensional photon gas in a dye microresonator [37]. Here a thermal contact between photons and a dye solution working as a heat bath is achieved. This leads to a thermalization of the transversal photon state. Signatures of this thermalization process are Bose-Einstein distributed photon energies and a spatial relaxation of the photon gas induced by an effective trapping potential. Once the phase space density approaches a value of order unity Bose-Einstein condensation to the transversal ground mode can be observed [38]. It is one of the purposes of this paper to give a more detailed account on the experiments we have performed so far. In section II we describe the basic ideas behind the experiment, together with a rate equation model describing the thermalization. In section III the experimental apparatus is described. The experimental results obtained concerning the thermalization of the photon gas are presented in section IV, followed by a detailed account on the experiments on Bose-Einstein condensation of photons in section V. We conclude the paper with an outlook on possible future directions for the photonic BEC.

II. EXPERIMENTAL SCHEME

In our experiment we use a bispherical microresonator filled with a drop of a dye solution, see Fig. 1. By multiple fluorescence and reabsorption the photon gas gets in thermal contact with the dye solution, and takes over its temperature, which in our case is room temperature. This thermalization process of the photon gas stems from a thermalization process of the rovibronic dye state. Due to frequent collisions, on a femtosecond timescale at room temperature, with the molecules of the solvent the rovibronic dye state is permanently altered. These processes are fast enough that both absorption and emission of photons always take place from highly equilibrated rovibronic dye states. As a consequence the spectral distributions of absorption $\alpha(\omega)$ and fluorescence $f(\omega)$ are linked by the Boltzmann factor $f(\omega)/\alpha(\omega) \propto \omega^3 \exp(-\hbar\omega/k_B T)$. This relation is known as the Kennard-Stepanov relation [39–42]. Here $\alpha(\omega)$ is the absorption coefficient of the dye solution, and $f(\omega)$ is the average spectral energy density of an emitted photon in free space. By multiple absorption and emission processes this Boltzmann factor is transferred to the spectral distribution of the photon gas. This can be seen by investigating the corresponding rate equations for absorption and emission [43]. More precisely the photon gas thermalizes at the spectral temperature defined by

$$T_{\text{spec}}(\omega) = \frac{\hbar}{k_B} \left(\frac{\partial \ln \tilde{\alpha}(\omega)}{\partial \omega} \frac{1}{\tilde{f}(\omega)} \right)^{-1}, \quad (1)$$

where dimensionless profiles, $\tilde{\alpha}(\omega) = \alpha(\omega)/\alpha(\omega_0)$ and $\tilde{f}(\omega) = f(\omega)\omega^{-3}/f(\omega_0)\omega_0^{-3}$ for an arbitrary ω_0 , have been used [38]. However, this spectral temperature coincides for a variety of dye molecules with the thermodynamic temperature of the dye, $T_{\text{spec}}(\omega) \simeq T$, to good approximation. This is especially true for the dyes used in the experiment, rhodamine 6G and perylene diimide. Regarding the photon number, it is clear that the fluorescence induced thermalization process conserves the photon number on average. A dye molecule can only emit an optical photon from its electronically excited state if it has absorbed a photon before. A purely thermal excitation is largely suppressed at room temperature by a factor $\exp[-\hbar\omega_c/k_B T] \simeq 10^{-37}$ with $\hbar\omega_c \simeq 2.1$ eV. In contrast to a black body radiator, the number of (optical) photons in the cavity is not determined by the temperature of the dye solution. The chemical potential of the photon gas thus in general is non-zero. In the experiment, photons are injected into the cavity by means of an external pumping laser, whose power thus determines the chemical potential.

The mirror separation is in the micrometer regime, namely $D_0 \simeq 1.46 \mu\text{m}$ on the optical axis, and is of the order of the optical wavelength. Consequently, the free spectral range of the resonator, of order $\simeq 100$ nm, becomes comparable to the spectral width of the dye fluorescence. The presence of the mirrors modifies the spon-

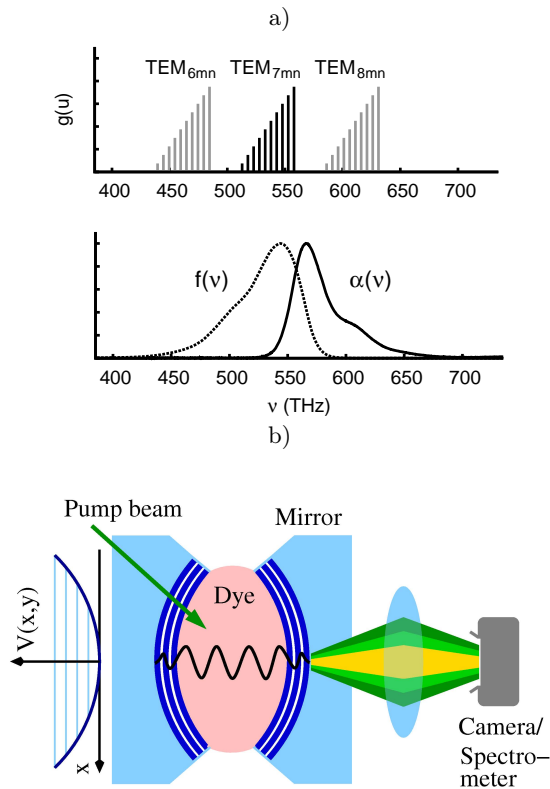


Figure 1: Experimental scheme. (a) Resonant modes of the microcavity (top) and relative absorption $\alpha(\nu)$ as well as fluorescence strength $f(\nu)$ for rhodamine 6G (bottom). The height of the bars indicates the degeneracy of the photon energy. Inside the microcavity, to a good approximation only fluorescence photons with a longitudinal wave number of $q = 7$ (black bars) exist, which causes this degree of freedom to be frozen out making the photon gas effectively two-dimensional. (b) Schematic set-up of the dye-filled microcavity. The curvature of the mirrors provides a trapping potential in the transversal plane, as indicated on the left. Photons with high transversal excitation numbers (green) are emitted at a larger angle to the optical axis, whereas transversally less excited radiation (yellow) exhibits a lower spatial divergence.

taneous emission from the excited molecules inside the cavity such that predominantly photons of a certain longitudinal mode number q are found to be emitted, typically $q = 7$ in our case. By this, one degree of freedom is frozen out and the photon gas becomes two-dimensional, as only the two transversal mode numbers are variable. Moreover, this establishes a ground state for the photons with non-vanishing energy - the transversal ground mode TEM _{$q00$} . In thermal equilibrium, the transversal excitations are expected to be Bose-Einstein distributed. Consequently, for increasing temperature of the dye solution, the average angle of propagation of the photons with respect to the optical axis will increase, while for low temperatures the photons are expected to propagate nearly parallel to the optical axis.

A. Cavity photon dispersion

Formally, the photon gas can be mapped onto a two-dimensional, ideal Bose gas in a harmonic trapping potential. This can be seen by investigating the energy-momentum relation. The energy of a photon as a function of longitudinal wave number k_z and transversal wavenumber $k_r = \sqrt{k_x^2 + k_y^2}$ is given by

$$E_{\text{ph}} = \frac{\hbar c}{n} \sqrt{k_z^2 + k_r^2}, \quad (2)$$

where n is the index of refraction of the medium. Due to the mirror curvature the boundary conditions for the photon modes (in z -direction) depend on the distance from the optical axis $r = |\vec{r}|$. For simplicity these boundary conditions are taken to be metallic. For the longitudinal wavenumber $k_z = k_z(r)$ one can make the ansatz

$$k_z(r) = q\pi/D(r), \quad (3)$$

where

$$D(r) = D_0 - 2(R - \sqrt{R^2 - r^2}) \quad (4)$$

is the mirror separation at a distance r from the optical axis and R is the radius of curvature of the mirrors. To incorporate a possible nonlinear photon interaction we moreover allow the index of refraction of the medium to vary in space $n = n(\vec{r}) = n_0 + \Delta n_r$, with $\Delta n_r = n_2 I(\vec{r})$, in the presence of the light field. Here n_0 and n_2 are the linear and nonlinear indices of refraction of the medium, respectively, and $I(\vec{r})$ is the intensity. A non-zero value for n_2 can arise e.g. from a Kerr-nonlinearity or from thermo-optical effects. With that we derive

$$\begin{aligned} E_{\text{ph}}(\vec{r}, k_r) &= \frac{\hbar c}{n(\vec{r})} \sqrt{k_z^2(r) + k_r^2} \\ &= \frac{\hbar c}{n_0 + \Delta n_r} \sqrt{\left(\frac{q\pi}{D(r)}\right)^2 + k_r^2} \\ &\simeq \frac{\pi \hbar c q}{n_0 D_0} + \frac{\hbar c D_0}{2\pi n_0 q} k_r^2 + \frac{\pi \hbar c q}{n_0 D_0^2 R} r^2 - \frac{\pi \hbar c q}{n_0^3 D_0} \Delta n_r \end{aligned} \quad (5)$$

where in the last step both the paraxial approximation ($r \ll R$, $k_r \ll k_z$) and $\Delta n_r \ll n_0$ has been applied. For an effective photon mass defined by

$$m_{\text{ph}} = \frac{\pi \hbar n_0 q}{c D_0} = \frac{\hbar n_0}{c} k_z(0), \quad (6)$$

and a trapping frequency

$$\Omega = \frac{c}{n_0 \sqrt{D_0 R/2}}, \quad (7)$$

equation (5) can be written as

$$E_{\text{ph}}(\vec{r}, k_r) \simeq \frac{m_{\text{ph}} c^2}{n_0^2} + \frac{(\hbar k_r)^2}{2m_{\text{ph}}} + \frac{m_{\text{ph}} \Omega^2}{2} r^2 - \frac{m_{\text{ph}} c^2}{n_0^3} n_2 I(\vec{r}), \quad (8)$$

When the interaction term is omitted, i.e. for $n_2 = 0$, this is the energy-momentum relation of a non-relativistic, massive particle in two dimensions, bound by a harmonic trapping potential. The standard quantization procedure then leads to the well known energy spectrum of the bi-spherical resonator [44], with the energy levels equidistantly separated by $\hbar\Omega$ and the degeneracy increasing linearly. After rescaling the energy such that the lowest harmonic oscillator mode has zero energy, and defining the transversal photon energy $u = E_{\text{ph}} - m_{\text{ph}}c^2/n_0^2 - \hbar\Omega$ the degeneracy can be written as

$$g(u) = 2(u/\hbar\Omega + 1). \quad (9)$$

The prefactor 2 here goes back to the two-fold polarization degeneracy.

B. Statistical theory of the photon gas

The thermodynamics of such a system is well known: a harmonically confined two-dimensional Bose gas shows a phase transition to a BEC at low temperatures or high particle numbers [45–48]. The average occupation number of a certain transversal energy u is given by the Bose-Einstein distribution

$$n_{T,\mu}(u) = \frac{g(u)}{e^{\frac{u-\mu}{k_B T}} - 1}, \quad (10)$$

where the chemical potential of the photons is implicitly defined by

$$N_{\text{ph}} = \sum_u n_{T,\mu}(u), \quad (11)$$

with N_{ph} as the total (average) photon number. With that, the number of photons in the transversally excited resonator states is seen to saturate at a critical particle number N_c given by [45–48]

$$N_c \simeq \frac{\pi^2}{3} \left(\frac{k_B T}{\hbar\Omega} \right)^2. \quad (12)$$

If the total photon number is increased beyond this bound, a macroscopic fraction is expected to condense into the transversal ground state. In our experiments, the trapping frequency is of order $\Omega \simeq 10^{11}$ Hz, which is roughly 9 orders of magnitude higher than for experiments with ultracold atomic gases. At room temperature, $T = 300$ K, this gives a critical photon number of magnitude $N_c \simeq 10^5$, which is experimentally feasible. In principle, it would also be possible to lower the temperature of the dye solution below the critical temperature,

$$T_c \simeq \frac{\sqrt{3}\hbar\Omega}{\pi k_B} \sqrt{N_{\text{ph}}} = \frac{\sqrt{6}\hbar c}{\pi k_B n_0} \sqrt{\frac{1}{D_0} \frac{N_{\text{ph}}}{R}}, \quad (13)$$

to trigger the condensation for a fixed photon number. However, this is experimentally much more demanding.

Strictly speaking, phase transitions can only occur in the thermodynamic limit. From eq. 13 we see that this thermodynamic limit has to be $N_{\text{ph}} \rightarrow \infty$, $R \rightarrow \infty$ with $N_{\text{ph}}/R = \text{const}$, as only this retains T_c . A limit invoking $D_0 \rightarrow \infty$ is unphysical because the two-dimensionality of the photon gas will be lost. Other than in the confined case considered here, there is no thermodynamic limit for a macroscopic ground state occupation at finite temperatures for the homogeneous two-dimensional Bose gas [45–48]. Correspondingly, such a system is always multi-mode in the thermodynamic limit.

In contrast to polariton experiments [31–36], no strong atom-light coupling takes place in our experiment. The frequent collisions with the molecules of the solvent leads to a rapid decoherence of the dye state, i.e. the decoherence rate is bigger than the Rabi frequency. This prevents a coherent energy exchange between photonic and molecular excitations [49, 50]. Consequently, the eigenstates of the system are best described by the uncoupled photonic and molecular degrees of freedom. At any given point in time a certain number of photons, N_{ph} , and excited dye molecules, N_{exc} , populate the cavity. In a stationary state, i.e. no net flux, the ratio of these numbers will be linked by the ratio of the lifetimes of both species, $N_{\text{exc}}/N_{\text{ph}} \simeq \tau_{\text{exc}}/\tau_{\text{ph}}$. The lifetime of a photon τ_{ph} here denotes the average time between emission and reabsorption in the medium. For typical experimental parameters τ_{ph} is of magnitude 10 ps. The lifetime of the excited dye molecules τ_{exc} is well known to get modified by the presence of the cavity with respect to its free space value [51–59]. Its exact value has a complicated dependence on the detailed experimental conditions. Moreover, it will be influenced by the presence of other photons due to stimulated emission. Nevertheless, we expect it to be of order 1 ns for the used optical powers, and thus it remains clearly bigger than the photon lifetime under typical experimental conditions [54, 55]. As a result, the number of excited molecules will also be much bigger than the number of photons. This situation is best described by a grandcanonical particle exchange, where the photon gas exchanges particles with the reservoir of excited dye molecules. The question regarding the suitable statistical ensemble is important because the fluctuations of the photon number - and with that the coherence properties of the light - will strongly depend on the statistical ensemble, even in the thermodynamical limit [60–62].

C. Rate equation model

Semiclassical laser theory builds upon rate equation models, where laser action is predicted when the gain from stimulated emission exceeds the total loss [10]. In an analogous way we use a multimode theory based on rate equations to describe the thermalization in the here investigated dye-filled optical microcavity. The dye molecule is modelled by a Jablonski energy level scheme [63] commonly used in the Kennard-Stepanov theory of

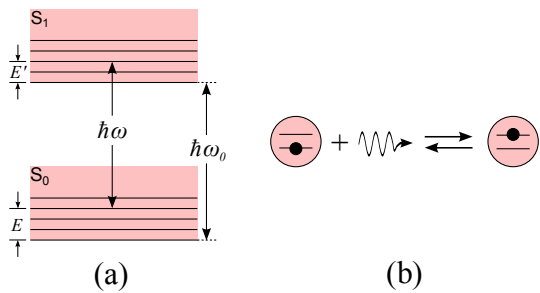


Figure 2: (a) Energy level scheme of a dye molecule with an electronic ground state S_0 and an excited state S_1 respectively, where "S" denotes singlet, which are separated by an energy $\hbar\omega_0$. Photons of a frequency ω are emitted and absorbed from within the rovibrational substates E and E' respectively. (b) Chemical reaction type exchange between different particle species, namely ground state dye molecules, photons and excited dye molecules.

absorption and emission [39–42, 64]. The present calculation neglects cavity specific modifications of the light-matter interaction, as well as fluctuations of the particle number, both issues that will be incorporated in a subsequent publication [65].

Consider a system with one ground and one excited electronic state, each with a manifold of rovibrational substates, see Fig. 2a. Let $\hbar\omega_0$ denote the energy splitting between the lowest rovibronic states (zero-phonon line). Furthermore, E and E' are considered to be rovibrational energies of ground and excited state and $\rho(E)$, $\rho'(E')$ denote the corresponding rovibronic densities of states. The distribution functions $p(E)$, as well as $p'(E')$, are proportional to the probability of finding a rovibronic state with energy E and E' ; for example $p(E) = \exp(-E/k_B T)$. With this, we expect the following total rates for spontaneous emission, stimulated emission and absorption of a photon at frequency ω :

$$R_{\text{spont}}(\omega) = \int dE' n_e(E') A(E', \omega), \quad (14a)$$

$$R_{\text{stim}}(\omega) = \int dE' n_e(E') B'(E', \omega) u(\omega), \quad (14b)$$

$$R_{\text{abs}}(\omega) = \int dE n_g(E) B(E, \omega) u(\omega), \quad (14c)$$

where $u(\omega)$ is the spectral energy density per unit volume of the radiation field, A , B and B' are the corresponding Einstein coefficients, and the occupation densities $n_e(E')$ and $n_g(E)$ of the excited and ground state populations are given by

$$n_e(E') = N_e \frac{\rho'(E') p'(E')}{W'}, \quad (15a)$$

$$n_g(E) = N_g \frac{\rho(E) p(E)}{W}. \quad (15b)$$

Here N_g and N_e denote the number of molecules in ground and excited states in the optically active volume. Further, W and W' are statistical weights given by

$W = \int dE \rho(E) p(E)$ and $W' = \int dE' \rho'(E') p'(E')$. This treatment assumes that cavity mirror losses and the coupling to unconfined optical modes are small, i.e. the rates associated with the corresponding loss processes are small compared to the processes accounted for in (14a)–(14c). Similarly, the rate for pumping, which compensates for these losses, will then be small. These conditions will be valid if a photon collides several times with dye molecules in the cavity before being lost, as can be achieved by re-absorption, i.e. by recapturing fluorescence.

The Einstein coefficients are not independent, their connection is given by

$$A(E', \omega) dE' = \hbar\omega D(\omega) B'(E', \omega) dE', \quad (16)$$

(A-B relation), with $D(\omega)$ as the spectral mode density per unit volume, and by

$$\rho'(E') B'(E', \omega) dE' = \rho(E) B(E, \omega) dE, \quad (17)$$

which follows from a detailed balance argument [64]. If we assume that the rovibrational dye state is in thermal equilibrium in both the electronic ground and excited states manifold respectively, which for many dyes is a reasonable assumption given that the typical time for a collision with solvent molecules is in the femtosecond regime at room temperature, while the electronic lifetimes are typically of the order of a nanosecond [63], we can apply Boltzmann distributions for $p(E)$ and $p'(E')$.

From the rate equations (14a)–(14c) the net variation of the photon number $n(\omega)$ at frequency ω is

$$\frac{dn(\omega)}{dt} = R_{\text{spont}}(\omega) + R_{\text{stim}}(\omega) - R_{\text{abs}}(\omega) \quad (18a)$$

$$= \int dE \rho(E) e^{-E/k_B T} B(E, \omega) \times \left[\frac{1}{W'} N_e e^{-\hbar(\omega-\omega_0)/k_B T} [\hbar\omega D(\omega) + u(\omega)] - \frac{1}{W} N_g u(\omega) \right], \quad (18b)$$

where in the second step we have used the energy conservation relation $\hbar\omega + E = \hbar\omega_0 + E'$ and the equations (16) and (17) to combine all integrals.

In a steady state, $dn(\omega)/dt = 0$, the term in squared brackets must vanish. This yields the equilibrium photon energy distribution

$$n(\omega) = \frac{g(\omega)}{\frac{N_g W'}{N_e W} e^{\hbar(\omega-\omega_0)/k_B T} - 1}, \quad (19)$$

where additionally $n(\omega) = \int dV \frac{u(\omega)}{\hbar\omega}$ and $\int dV D(\omega) = g(\omega)$, see eq. (9), were employed. In chemical equilibrium, the chemical potentials of all species are linked by $\mu_{\text{ph}} + \mu_g = \mu_e$ (Fig. 2b), where μ_{ph} is the chemical potential of the photons and μ_e , μ_g are the chemical potentials of excited and ground state dye molecules, respectively. From this one can easily show [65] that the fugacity of

the photons is determined by the excitation level in the dye medium

$$e^{\mu_{\text{ph}}/k_{\text{B}}T} = \frac{N_e W}{N_g W'} e^{\hbar\omega_0/k_{\text{B}}T}, \quad (20)$$

or, if we use a renormalized chemical potential $\mu = \mu_{\text{ph}} - \hbar\omega_c$,

$$e^{\mu/k_{\text{B}}T} = \frac{N_e W}{N_g W'} e^{\hbar(\omega_0 - \omega_c)/k_{\text{B}}T}. \quad (21)$$

Thus, in accordance with the usual convention, the photon number approaches infinity, $N_{\text{ph}} \rightarrow \infty$, for a vanishing chemical potential, $\mu \rightarrow 0$ with $T = \text{const.}$ When we combine the equations (19) and (21), we arrive at the Bose-Einstein distribution, eq. (10).

As it is well known from laser theory [10], the rate equations (14a)–(14c) do not allow for an inversion of a specific transition, and one therefore has to include a pumping term to the equations to model lasing. However, the rate equations do predict thermally distributed photon energies for certain conditions, as we have shown. This includes that the statistical weight of the resonator ground mode can become macroscopic. Put differently, 'single mode'-behaviour can arise even in thermal equilibrium and without inversion. This point is however only revealed in a statistical multi-mode treatment and is missed in the usual laser theory. That the photon condensate can arise in a non-inverted medium can also be understood by the capability of our system to reuse spontaneous emission. In a macroscopic laser reabsorption nearly inevitably leads to photon loss due to spontaneous emission into non-confined modes. However, if spontaneous emission is directed into the cavity, where it gets reabsorbed, the excitation will not be lost. Therefore spontaneous emission in general is not a loss channel in our system. Recapturing of fluorescence (or photon recycling) is a mechanism also known for "zero threshold" microlasers [66–68]. In those works one tries to capture spontaneous emission into a single cavity mode, while in the present scheme it is sufficient if the spontaneous photons are directed into one of the (many) transversal modes. The thermalization process will select the resonator ground state to have the biggest statistical weight, which can even be macroscopic, when condensation sets in.

III. EXPERIMENTAL SETUP

The experimental setup, as shown in Fig. 3, consists of a microresonator, a pump source and an analyzing section. The microresonator is formed by two highly reflecting, spherically curved, dielectric mirrors which are typically used for cavity ring-down spectroscopy. Their reflectivity is bigger than 0.99997 for the wavelength region (500 – 590) nm, with a reflectivity maximum of 0.999985 at $\lambda \approx 535$ nm. The latter corresponds to a finesse of

$F \approx 200000$ for the empty cavity. Two different radii of curvatures are available, $R = 1$ m and $R = 6$ m, respectively. To allow for a mirror separation of a few halfwaves on the optical axis despite the curvature, one of the mirrors is cut to a surface area of 1 mm × 1 mm. The edges are carefully polished to minimize possible stress from contact points between the mirrors. To verify that the mirror's reflectivity remains unaffected by the cutting and subsequent polishing procedure cavity ring-down measurements have been performed.

The microresonator is pumped at an angle of 45° with respect to the optical axis. At this angle and for a certain polarisation the mirrors show their first reflectivity minimum allowing a pump beam transmission of over 80%. To pump the resonator in this way is advantageous because resonance conditions and mode matching do not have to be considered. The pump beam can be placed at an arbitrary position inside the resonator plane independent of the cavity resonances. One of the mirrors is mounted on a translation stage with a piezoelectric actuator to allow fine tuning of the mirror separation, which can be computer-controlled to achieve an electronic stabilization. For that the fluorescence spectra emitted from the cavity are captured by a spectrometer and are used as an input for the stabilization protocol that controls the voltage driving the piezoelectric actuator. The bandwidth of this control loop is sufficient to compensate thermally induced fluctuations of the cavity length. Faster fluctuations are reduced by mechanically decoupling the cavity from the optical table and by the damping caused by the dye solution between the mirrors.

The used dyes are either rhodamine 6G or perylene-diimid (PDI), whose absorption and fluorescence spectra are shown in Fig. 4. The dyes show a quantum efficiency close to unity in the used spectral region, $\Phi_{\text{R6G}} \approx 0.95$ [69] and $\Phi_{\text{PDI}} \approx 0.97$ [70], and have spectral temperatures close to the thermodynamic temperature of the surrounding solvent, $T_{\text{spec}}(\omega) \simeq T$. For rhodamine we either use methanol or ethylene glycol as solvent, for PDI acetone is used. Repeated filtering of the solutions is necessary to remove unsolved dye particles and other contaminations. This filtering has proven to be crucial for the reliability of the experiment. To achieve reabsorption of the microcavity radiation fairly high concentrated dye solutions have to be employed. In principle high dye concentrations can lead to radiationless deactivation. However, the concentration used here, 1.5×10^{-3} Mol/l for rhodamine 6G, is still one order of magnitude lower than the concentration where fluorescence quenching notably sets in [71–73]. As pump source we use a frequency doubled Nd:YAG laser at a wavelength of 532 nm which is switched by two acousto-optic modulators operating in series to ensure a high on/off contrast. The analysis is performed by a spectrometer and a camera. For that the emitted radiation is split by a non-polarizing beam splitter. One part of the beam is mapped by an imaging system onto the chip of a color CCD camera, where a magnified real image of the photon gas is generated. The

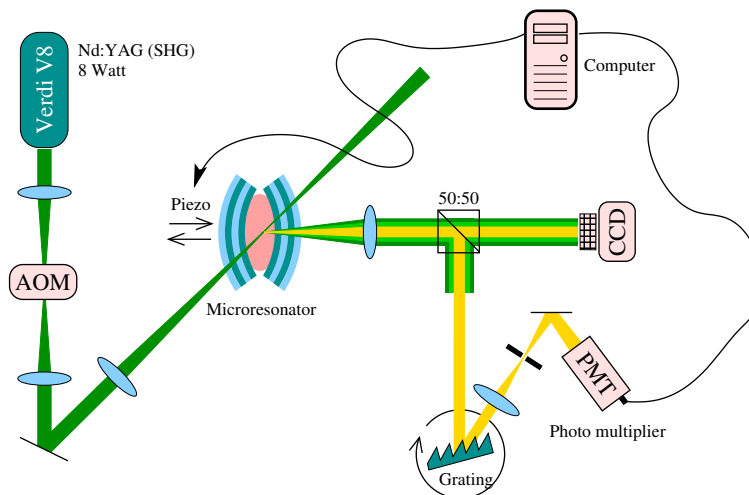


Figure 3: Schematic set-up of the microcavity experiment. The microresonator is pumped at an angle of 45° to the optical axis. The radiation emerging from the microresonator is examined both spatially and spectrally.

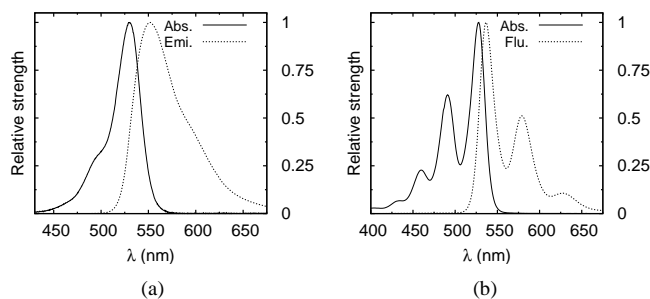


Figure 4: Relative strengths of absorption $\alpha(\lambda)/\alpha_{\max}$ and fluorescence $f(\lambda)/f_{\max}$ for the dyes (a) rhodamine 6G and (b) perylene diimide.

other part of the beam is directed into a spectrometer. We use either a commercially available one, with optical resolution $\simeq 2$ nm, or a self-built spectrometer. Care has to be taken when the spectrometer has an entry slit, as it is the case for the commercial spectrometer, where the width is $15 \mu\text{m}$. Due to their bigger mode diameter and higher divergence the coupling of higher transversal modes through the slit typically will be much less efficient than, for example, for the ground mode TEM_{q00} . Consequently, the entry slit will not be neutral in color anymore. One way to overcome this problem is to use a diffusing plate in the light path that cancels out the correlation between position, angle and color. A more advantageous way is to omit the entry slit altogether and to directly pass the light onto a diffractive grating. This is possible because the emitted radiation from the microcavity is only weakly divergent and can be sufficiently collimated before being spectrally decomposed. This scheme is realized in our self-built spectrometer, using a rotating diffractive grating with 2400 lines/mm and a photomultiplier tube as detector. However, both methods described above deliver largely equivalent spectra.

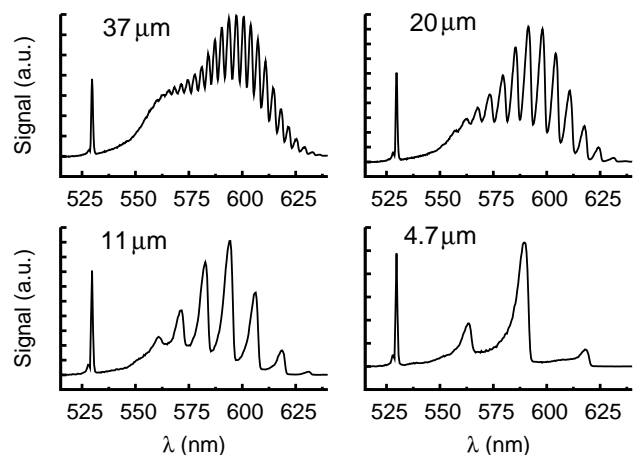


Figure 5: Spectral distribution of the radiation emitted from the microcavity for different mirror separations, $D \approx \{37, 20, 11, 4.7\} \mu\text{m}$, corresponding to different cavity orders $q \approx \{175, 95, 50, 22\}$. (Rhodamine 6G in methanol, $\varrho = 1.5 \times 10^{-3} \text{ Mol/l}$, mirror curvatures $R_1 = 1 \text{ m}$ and $R_2 = 6 \text{ m}$)

IV. THERMALIZATION OF THE TRANSVERSAL PHOTON STATE

A. Spectral and spatial photon distribution

Figure 5 shows typical spectral distributions of the emitted microresonator light for decreasing mirror separation (from upper left to lower right). By investigating the free spectral range the longitudinal mode number of the photons can be determined. For very small mirror separations a regime is reached where the photon gas gets two-dimensional, i.e. where only photons of a single longitudinal mode number are emitted. The shortest mirror separation that can be reached in our experiment

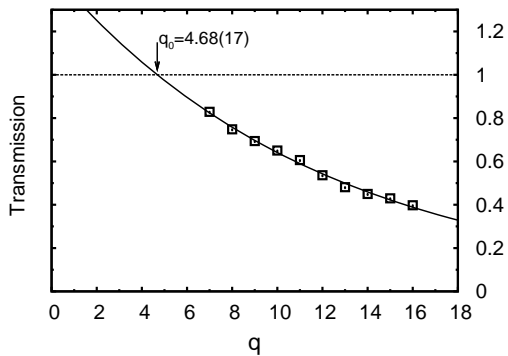


Figure 6: Transmission of the pump beam (squares) as a function of the longitudinal mode number q . The solid line corresponds to the Lambert-Beer law $I(q)/I_0 = \exp(-\alpha(q - q_0)\lambda_c/2n_0)$ with the fitting parameter $q_0 = 4.68 \pm 0.17$. This measurement shows that the effective end nodes of the optical resonance are located inside the mirrors. (Rhodamine 6G in methanol, $\rho \approx 2 \times 10^{-2}$ Mol/l, mirror curvatures $R_1 = R_2 = 1$ m)

corresponds to $q = 7$ halfwaves. The limiting factor that prevents a further reduction of q is the penetration of the light field into the mirror material. This can be seen by determining the transmission coefficient of the pump light, which is illustrated in Fig. 6. For this measurement very high concentrated dye solutions are used (rhodamine 6G at 2×10^{-2} Mol/l). As expected, the transmission of the pump light shows an exponential decay with increasing q (Lambert-Beer law). However, the decay curve extrapolates to full transmission at a value of $q_0 = 4.68 \pm 0.17$. Apparently the thickness D_{dye} of the dye film is not directly proportional to q but shows an offset, following $D_{\text{dye}}(q) \propto (q - q_0)$. For example, the dye film thickness at $q = 7$ is just over two halfwaves. The effective end nodes of the light field are located about 2.3 halfwaves (corresponding to 400 – 450 nm) inside the mirrors. Longitudinal mode numbers $q < 5$ are therefore not possible with the used mirrors.

The true ground state of the resonator is the halfwave resonance TEM_{100} . The freezing out of the longitudinal mode number at mirror separations corresponding to $q \gtrsim 7$ is not obvious at first sight. Fluorescence into $\text{TEM}_{8\text{mn}}$ modes, or into transversally low excited $\text{TEM}_{6\text{mn}}$ modes are energetically excluded due to the finite spectral width of the dye emission. But fluorescence into transversally high excited $\text{TEM}_{6\text{mn}}$ modes is energetically possible. However, due to their much higher mode volume and consequently smaller overlap with an emitting point dipole, decays into higher $\text{TEM}_{6\text{mn}}$ modes are expected to be much slower than emission processes into the energetically equivalent but transversally low excited $\text{TEM}_{7\text{mn}}$ modes. This is indeed also seen in the experimental spectra (Fig. 5), where a preference for low transversal modes is already seen for rather large mirror separations. Thus mode hopping to longitudinally lower excited modes is not found to be a relevant loss mecha-

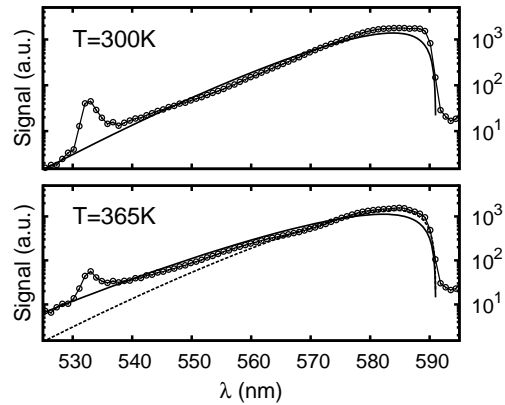


Figure 7: Spectral distribution of the radiation emitted from the microcavity far below the critical photon number at $T = 300$ K and $T = 365$ K (circles). The spectra are in good agreement with the Boltzmann-distributed photon energies (lines). For comparison a $T = 300$ K Boltzmann-distribution is additionally plotted in the bottom graph (dashed line). (Rhodamine 6G in ethylene glycol, $\rho = 5 \times 10^{-4}$ Mol/l, mirror curvatures $R_1 = R_2 = 1$ m, $q = 7$)

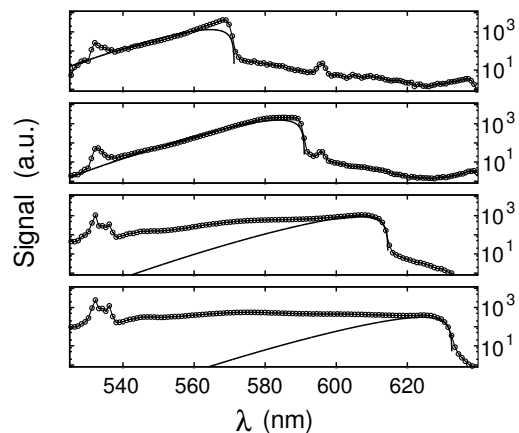


Figure 8: Normalized spectral distribution of the radiation emitted from the microcavity (circles) for 4 different cut-off wavelengths $\lambda_c \approx \{570, 590, 615, 625\}$ nm. In addition, Boltzmann-distributed photon energies for $T = 300$ K are plotted (lines). (Experimental parameters as in Fig. 7)

nism for the two-dimensional photon gas.

Measurements of the spectral photon distribution in the microresonator at room temperature, $T = 300$ K, and for a heated resonator setup at $T = 365$ K can be seen in Fig. 7. The power of the transmitted light is $P_{\text{out}} = (50 \pm 5)$ nW. From this value an average photon number of $N = 60 \pm 10$ inside the resonator can be derived. A numerical solution of eq. (11) then leads to a chemical potential of $\mu/k_B T = -6.76 \pm 0.17$ ($T = 300$ K) and $\mu/k_B T = -7.16 \pm 0.17$ ($T = 365$ K). These measurements are thus performed far from the phase transition that is expected to set in for μ getting close to zero. Consequently the term ‘-1’ in the denominator

of the Bose-Einstein distribution, eq. (10), can be neglected and the spectral distribution of the photons is expected to be Boltzmann-like. Besides some deviations around 532 nm caused by scattered pump light the measured spectra show a good agreement with the theoretical expectations both for $T = 300$ K and for $T = 365$ K, respectively. This can be interpreted as evidence for a thermalization process of the transversal photon state.

As stated before a thermalization process is expected to occur only if a thermal contact between photon gas and dye solution is achieved by reabsorption. To verify this experimentally we varied the cut-off wavelength $\lambda_c = 2\pi c/\omega_c$ by tuning the piezo voltage, as is shown in Fig. 8. For smaller λ_c the absorption coefficient of the dye solution gets bigger and consequently the emitted photons are reabsorbed faster. Thus a sufficient thermal contact is expected to remain in this case. The upper curves in Fig. 8 confirm this (note the logarithmic intensity scale). The thermal drop-off of the transversal excitations is indeed visible. This does not hold anymore if λ_c is moved to a larger wavelength, see the lower two spectra in Fig. 8. Here the absorption coefficient is not big enough to achieve reabsorption and consequently the spectra differ quite strongly from a Boltzmann distribution. A similar observation can also be made by varying the dye concentration. For low dye concentrations the spectra are only partially thermalized.

Not only the spectral but also the spatial photon distribution shows the expected characteristics of a thermal gas. In Fig. 9a a picture of the photon gas taken by a color CCD camera is shown. For that the photon gas was mapped with a lens system as a magnified real image onto the CCD chip. Transversally low excited photons (yellow) are seen in the direct vicinity of the trap centre while the highly excited photons (green) oscillate stronger in the transversal plane. From this picture the spatial distribution of the photons, here a cut along an axis through the centre, can be determined, see Fig. 9b. Additionally the theoretical thermal expectation value, which far below criticality is given by a Gauss distribution, is plotted here (solid line). The good agreement between the two curves again confirms the thermal character of the photon gas. This is however not unexpected as the spectral distribution of the photons has already revealed Boltzmann-like statistical weights and spectral and spatial distributions can be mapped onto each other in a thermalized system.

B. Redistribution of photons

To further characterize the thermalization process we investigated the influence of the pump beam position. For that the pump beam is displaced with respect to the optical axis. Due to the thermalization process we nevertheless expect the photons to accumulate in the trap centre where their potential energy is minimized. The result of such a measurement can be found in Fig. 10.

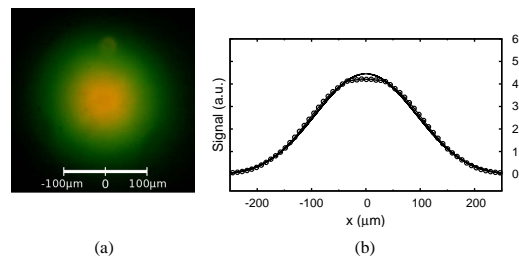


Figure 9: (a) Picture of the photon gas (real image onto the sensor of a color CCD camera). Low-energy photons (yellow) are emitted from the direct vicinity of the trap centre, while the emission of higher-energetic photons (green) occurs outside of the centre. (b) Photon distribution along an axis intersecting the trap centre (circles), extracted from Fig. 9(a). The theoretical distribution function (line) is based on a thermal averaging over all resonator modes and it corresponds to a Gaussian distribution. (Experimental parameters as in Fig. 7)

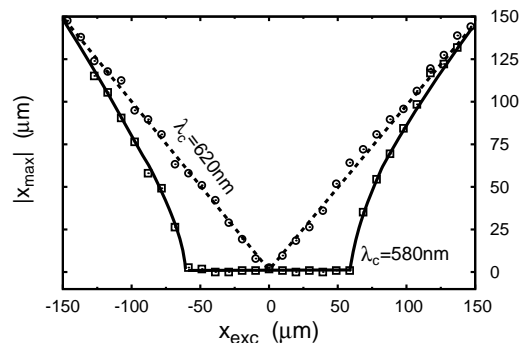


Figure 10: Measured distance of the intensity maximum of the emitted fluorescence from the trap centre, $|x_{\max}|$, as a function of the position of the excitation spot, x_{exc} . For a cut-off wavelength of $\lambda_c = 620$ nm, corresponding to weak reabsorption, the fluorescence exactly follows the pump spot (circles connected by dashed line), for $\lambda_c = 580$ nm, corresponding to strong reabsorption, the photons concentrate to the trap centre, $x_{\max} = 0$, provided the pump spot is displaced less than $60 \mu\text{m}$ from the trap centre (squares connected by a solid line). (PDI in acetone, $\rho = 0.75$ g/l, mirror curvatures $R_1 = R_2 = 1$ m, $q = 7$)

In this figure the distance of the fluorescence maximum from the optical axis as a function of the pump position is shown. The pump spot is stepwise moved along a line through the centre and at every position x_{exc} the distance between the point of brightest fluorescence and the optical axis $|x_{\max}|$ is measured. The diameter (fwhm) of the pump spot is roughly $25 \mu\text{m}$. These measurements are performed for two different cut-off wavelengths λ_c . At $\lambda_c \approx 620$ nm reabsorption of the fluorescence light is nearly absent due to the much smaller absorption coefficient in this spectral regime and the decreasing mirror reflectivity. Consequently the photons leave the cavity in the direct vicinity of the pump spot and the opposite turning point, i.e. pump spot and absolute value of the position of the intensity maximum are nearly identical.

For $\lambda_c \approx 580$ nm reabsorption is strong enough to trigger the thermalization process. Here the majority of photons can accumulate in the potential minimum before they get lost. However, this only holds if the position of the pump beam is not too far away from the optical axis. This maximum distance is determined to be roughly $\simeq 60$ μm for the given experimental conditions. If the pump spot is moved beyond that radius, the photon gas does not reach its equilibrium spatial distribution anymore. The loss of spatial thermalization is accompanied by a non-thermal spectral distribution. We interpret this observed spatial redistribution effect as further evidence for the presence of a thermalization process.

The reason for the incompleteness of the thermalization process for stronger displaced pump spots is attributed to the finite number of emission-reabsorption cycles a photon can undergo on average before it is lost. For larger displacements this number apparently is insufficient to reach the equilibrium spatial distribution of the photon gas. We expect the most important loss channel to be the coupling to unconfined modes. The mirrors used in the experiments show a drop-off in reflectivity for angles larger than 45° . At every emission process therefore a non-negligible probability exists that a photon is scattered out of the cavity. Mirrors with a full three dimensional bandgap would certainly improve on this [74, 75]. A second loss channel is radiationless deactivation. The average number of emission-reabsorption cycles is bounded by the quantum efficiency smaller than unity. This average is given by $\sum_{n=0}^{\infty} \Phi^n (1 - \Phi) n = \Phi / (1 - \Phi)$. For rhodamine 6G ($\Phi_{\text{R6G}} = 0.95$) it corresponds to 19 fluorescence processes, for PDI ($\Phi_{\text{PDI}} = 0.97$) it is 32. Both numbers seem to be rather big and we therefore do not expect the finite quantum efficiency to be the dominant loss mechanism. This is especially true because the quantum efficiencies could even improve compared to the free space values we have stated above. Such an effect is expected if the lifetime of the excited molecules is shortened due to modified spontaneous emission within the cavity.

V. BOSE-EINSTEIN CONDENSATION

A. Spectral and spatial photon distribution

We now describe the behaviour of the photon gas for higher intracavity powers. For these experiments the resonator is pumped with powers of $P_{\text{pump}} \gtrsim 100$ mW. However during the one-time pass of the pump beam through the cavity only a small fraction of the light is actually absorbed in the dye film - less than 1 mW, the remainder is simply transmitted. To prevent excessive population of dye triplet states and heat development, the pump light is chopped into rectangular pulses of 0.5 μs duration. The duty cycle is typically 1:16000, i.e. every pulse is followed by a dark phase of 8 ms duration. For pulse durations longer than 0.5 μs the intracavity power is ob-

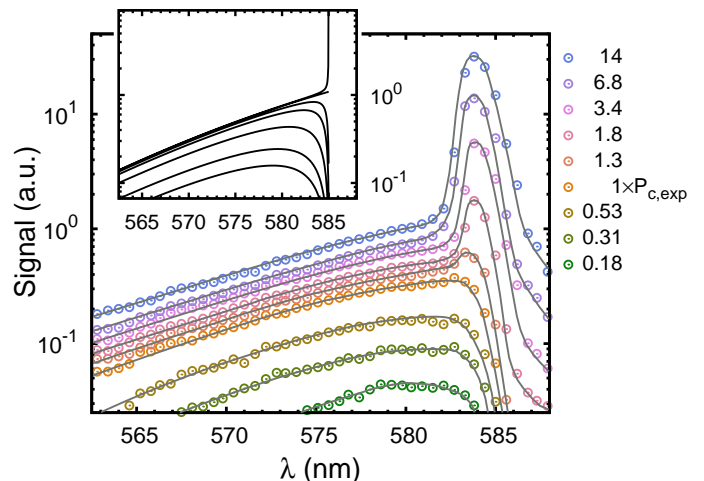


Figure 11: Spectral photon distribution for increasing intracavity power. The optical powers are normalized to the experimentally determined critical power $P_{c,\text{exp}} = (1.55 \pm 0.60)$ W, which corresponds to a critical photon number of $N_c = (6.3 \pm 2.4) \times 10^4$ (Rhodamine 6G in methanol, $\varrho = 1.5 \times 10^{-3}$ Mol/l, mirror curvatures $R_1 = R_2 = 1$ m, $q = 7$, pulse duration 0.5 μs). The inset features theoretical spectra based on a Bose-Einstein distribution of the transversal excitations.

served to decay. We attribute this to the population of triplet states. This time scale is indeed also known for dye lasers as long as no triplet quenchers are used [76]. Since the pulses are at least two orders of magnitude longer than the lifetime of the excited state dye molecules and roughly four orders of magnitude longer than the lifetime of the photons, the experimental conditions can be considered quasi-static.

The experimentally observed spectral distributions of the cavity photons for increasing intracavity power is shown in Fig. 11. In the inset the theoretical spectra based on Bose-Einstein distributed transversal excitations at 300 K are depicted. The circulating light power inside the cavity is determined by measuring the transmitted power through one of the mirrors and using the transmission coefficient as the proportionality factor. As observed before, the spectral distribution is Boltzmann-like for low photon numbers. However for higher photon numbers the maximum of the distribution slightly shifts to larger wavelengths accompanied by a spectral narrowing. Beyond a certain critical value, a spectrally sharp peak near the cut-off appears. Due to the insufficient resolution of the spectrometer of ≈ 2 nm, it is not possible to decide from the spectra which mode is massively populated. Clear-cut evidence for the massive population of the ground mode is however provided by the spatial distribution shown in Fig. 12. The central bright spot visible has a diameter (fwhm) of (14 ± 2) μm . This corresponds well to the expected diameter of the transversal ground state $d_{\text{TEM}_{400}} = 2\sqrt{\hbar \ln 2 / m_{\text{ph}} \Omega} \simeq 12.2$ μm for the given experimental parameters. The experimentally determined critical light power inside the cavity is $P_{c,\text{exp}} \approx$

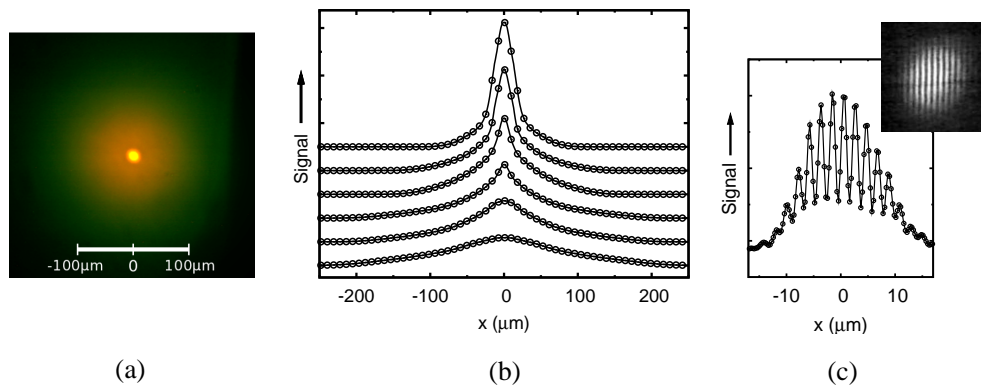


Figure 12: Picture of the photon gas (real image onto the sensor of a color CCD camera). Low-energy photons (yellow) are emitted from the direct vicinity of the trap centre, while the emission of higher-energetic photons (green) occurs outside of the centre. (b) Photon distributions along an axis intersecting the trap centre for increasing order parameter $N_0/N \approx \{0\%, 0\%, 1\%, 3\%, 10\%, 25\%\}$ (circles). (c) Interference pattern obtained by superimposing two partial beams of the condensate using a Michelson-interferometer. Here the path difference of the two interferometer arms is 15 mm. (experimental parameters as in Fig. 11)

(1.55 ± 0.60) W. If this value is normalized by the power per photon, $P_{\text{ph}} \simeq \hbar\omega_0/\tau_{\text{rt}}$, where τ_{rt} is the round trip time, one obtains a critical photon number of $N_{\text{c,exp}} \simeq P_{\text{c,exp}}\tau_{\text{rt}}/\hbar\omega_0 \approx (6.3 \pm 2.4) \times 10^4$. Within the quoted uncertainty, the value is in agreement with the theoretically expected number of $N_{\text{c}} = (\pi^2/3)(k_{\text{B}}T/\hbar\Omega)^2 \simeq 77000$ for the given parameter and thus confirms that the observed condensation phenomenon occurs at a particle number which is characteristic for a BEC. We have repeated the measurement for a different dye (perylene-diimide (PDI), 0.75 g/l in acetone). Since the only property of the dye that effects the condensation process should be its temperature, we do not expect the critical photon number to differ from the rhodamine case. This is indeed confirmed experimentally; within the given uncertainties no deviation of $P_{\text{c,exp}}$ or $N_{\text{c,exp}}$ is observed. There is however a difference regarding the pump power that is needed to achieve the critical photon number inside the resonator. The reason for this is the lower absorption coefficient of PDI at the pump wavelength of 532 nm. This is roughly a factor of 3 smaller than for rhodamine. To reach the same amount of absorbed pump power one therefore has to pump harder.

The relatively large uncertainties regarding $P_{\text{c,exp}}$ and $N_{\text{c,exp}}$ stem from a combination of mainly systematic error sources, especially uncertainties in the calibration of the power meter and in the transmission coefficient of the mirrors, $t = (2.5 \pm 0.4) \times 10^{-5}$. Moreover, since the cw-power coupled out at the phase transition is only of order ≈ 1 nW, care has to be taken that the power measurement is not falsified by scattered pump light or background fluorescence from the edges of the mirrors. Here a spatial filtering has proved to be helpful. However, one has to ensure that especially the higher transversal modes are not blocked by this filtering. At last it is also necessary that the spatial pump distribution, here a Gaussian ground mode with beam waist $2w_0 \approx 100 \mu\text{m}$ centered

around the optical axis, differs not too strongly from the equilibrium distribution of molecular excitations. As it already has been shown in the previous section, the photon gas does not reach its equilibrium state if this spatial mismatch gets too big. In this case a position dependence of the chemical potential remains that is not completely removed by the thermalization process before photons leave the cavity. Such a non-equilibrium situation will also influence the critical photon number.

To obtain the spatial photon distribution, pictures of the photon gas for various pump levels have been recorded and analyzed quantitatively. The intensity profiles (cut along an axis through the trap center) shown in Fig. 12b have been normalized to equal area and are shifted in the y-direction for the sake of visibility. These profiles show an increasing spatial concentration of the photons in the trap centre prior to the phase transition - a feature, which is in good agreement with the theoretically calculated intensity profiles. However, there is an interesting deviation of the experimental profiles from the theoretical ones; the experiments reveal an increase of the ground mode diameter with the ground state occupancy. This is not expected for an ideal gas of photons and thus indicates the presence of a repelling photon-photon interaction induced by the medium. Such an interaction could e.g. arise from a Kerr-nonlinearity of the dye molecules. However, in our case it seems to stem mainly from a thermo-optical effect, further investigations are presented in section 5.5. Another indication of the selfinteraction is the non-perfect saturation of the thermal modes, which can be attributed to a change in the effective trapping potential for higher occupation numbers [77].

Preliminary experiments regarding the coherence of the condensate have been performed. The light beam coupled out of the resonator is sent through a Michelson interferometer with a pathway difference of roughly 15 mm, see Fig. 12c. For this measurement the interfer-

ometer is slightly misaligned such that the two interfering beams do not propagate collinear. The resulting interference pattern demonstrates that the first order coherence of the condensate at least extends into the centimeter regime. However, a more thorough characterization of the coherence length is subject to ongoing experiments and will be presented in a subsequent publication.

B. Scaling of the critical power with the resonator geometry

The critical circulating power as a function of the geometry parameters of the resonator can be casted in the form

$$P_c \simeq \frac{\pi^2}{12} \frac{n_0 \omega_0}{\hbar c} (k_B T)^2 R. \quad (22)$$

One expects a linear increase of P_c with increasing radius of curvature R and no dependence on the longitudinal mode number q - at least as long as the two-dimensionality of the photon gas holds. To test the dependence on R , mirrors with two different curvatures are available, $R_1 = 1$ m and $R_2 = 6$ m, allowing three different mirror combinations. The combination $R_{\text{left}} = 1$ m and $R_{\text{right}} = 6$ m is equivalent to a resonator built from two identical mirrors with a radius given by the harmonic mean $R = 2(R_1^{-1} + R_2^{-1})^{-1} \simeq 1.71$ m. In Fig. 13a the experimentally determined values of the critical power as a function of the effective radius R are shown together with the theoretical expectation given by eq. (22). The data points coincide well with the theoretic prediction - both the linear scaling and the absolute values. Seen in another way, the procedure of increasing both the radius of curvature R and the photon number N but preserving the ratio R/N is observed to retain the critical temperature of $T_c = 300$ K. Thus, if this procedure was continued indefinitely, one could reach the thermodynamic limit for condensation at a finite temperature. In a further measurement we have investigated the dependence of the critical power P_c on the longitudinal mode number q . For that, q is increased stepwise without varying the cut-off wavelength $\lambda_c = 585$ nm, see Fig. 13b. As expected, q has no significant influence on P_c within the given experimental uncertainties. Both measurements again confirm that the observed condensation occurs at the BEC criticality condition.

Interestingly, transitions to lower longitudinal modes were not observed to be significant, which we attribute to the vanishing spatial overlap of the modes. The observed spectra indicate that the photon gas remains to good approximation two-dimensional up to a cavity length of at least 16 halfwaves. The pump power that is necessary to achieve the critical photon number shows a strong dependence on the mirror separation, see upper graph in Fig. 13b. If the longitudinal mode number is doubled from $q = 8$ to $q = 16$ by increasing the mirror separation, only one third of the initial pump power is necessary

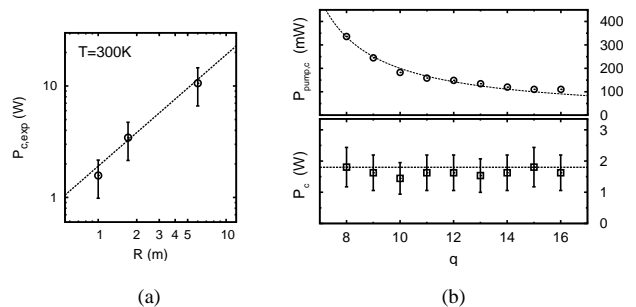


Figure 13: (a) Critical circulating intracavity power as a function of the effective mirror curvature R . (Rhodamine 6G in methanol, $\varrho = 1.5 \times 10^{-3}$ Mol/l, $q = 7$, pulse duration $0.5 \mu\text{s}$) (b) Pump power at the phase transition (top) and critical intracavity power (bottom), respectively, as a function of the cavity order q . (Rhodamine 6G in methanol, $\varrho = 1.5 \times 10^{-3}$ Mol/l, mirror curvatures $R_1 = R_2 = 1$ m, pulse duration $0.5 \mu\text{s}$)

to reach criticality. Thus the system shows a behaviour contrary to threshold behaviour reported for dye [66, 78] or semiconductor microlasers [67], where an increase of the threshold pump power with the cavity length has been observed. The reason for the here observed decrease of the pump power is an increase of the absorbance for thicker dye films. Since the observed critical circulating power P_c is independent of the cavity length, the absorbed pump power at criticality should also be roughly constant. Thus in the weak absorption limit, as in our case, one expects to see a reciprocal dependence of the pump power P_{pump} on the dye film thickness $D_{\text{dye}}(q)$, as this conserves the amount of absorbed pump power. Thus we expect $P_{\text{pump}} \propto (q - q_0)^{-1}$, with the penetration depth into the mirrors q_0 . The corresponding fit to the experimental data is shown in the upper graph of Fig. 13b. For the parameter q_0 one obtains a value of $q_0 = 4.77 \pm 0.25$, in good agreement with the value of $q_0 = 4.68 \pm 0.17$ derived in section 4.1 by directly measuring the absorbance. This confirms that the necessary absorbed pump power to trigger criticality remains constant for various mirror separations. The given values of the critical pump power can also be converted to pump intensities, $I_{\text{pump},c} = P_{\text{pump},c} / \pi w_0^2$, where $w_0 \simeq 50 \mu\text{m}$ is the pump beam radius. One obtains values roughly in the regime $(0.6 - 2.2) \text{ kW/cm}^2$, where the given values of $P_{\text{pump},c}$ in Fig. 13b have to be corrected by the mirror transmission coefficient, which is of order 50%. These values are roughly two orders of magnitude smaller than in macroscopic dye lasers, where typically pump intensities of order $\approx 100 \text{ kW/cm}^2$ are required [79, 80].

C. Condensation by spatial relaxation

As it was already demonstrated in section 4.2, the thermalization process is accompanied by a spatial redistribu-

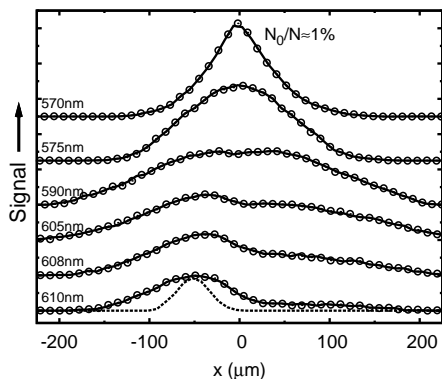


Figure 14: Intensity distribution of the photon gas along an axis intersecting the trap centre for varied cut-off wavelengths λ_c (left edge). The pump beam (dashed line) is located outside the trap centre and its position as well as its power are kept fixed during the measurement. The top curve shows a photon gas precisely at the phase transition with a ground state population $N_0/N \lesssim 1\%$. (Rhodamine 6G in methanol, $\varrho = 1.5 \times 10^{-3}$ Mol/l, mirror curvatures $R_1 = R_2 = 1$ m, $q = 7$, pulse duration 0.5 μ s)

tion of the photons towards the trap centre. This redistribution can also be observed for higher photon numbers. It can even provide a sufficiently high density at the trap centre to trigger the condensation. To demonstrate this, we have performed the following experiment: the dye solution is pumped 50 μ m away from the optical axis with a pump beam of roughly 35 μ m (fwhm) diameter. Both its position and its power are kept fixed in the course of the experiment. By fine tuning the cavity cut-off λ_c , we can vary the amount of reabsorption.

The lowest profile in Fig. 14 shows the intensity of the photon gas along a line through both trap centre and pump position for a cavity cut-off of $\lambda_c = 610$ nm. Additionally the profile of the pump spot alone is displayed, where thereto one of the cavity mirrors was removed. For this value of λ_c the degree of reabsorption is low and the thermalization process is suppressed. The observed spatial distribution of the photon gas roughly follows the pump beam intensity distribution. If λ_c is decreased, the amount of reabsorption is increased and the thermal contact between photon gas and dye solution is gradually established. The intensity profiles get distributed more symmetrically around the trap centre. For a cavity cut-off of $\lambda_c = 570$ nm the photon density in the centre even gets sufficiently high to trigger criticality. This is both indicated by a small bright spot occurring at the position of TEM₀₀-mode and the corresponding cusp in the intensity profile (upper curve in Fig. 14). However, the condensate fraction that is achieved in this way is rather low, $N_0/N \lesssim 1\%$.

An important conclusion from this measurement is that the condensation is triggered not directly by the pumping. The intensity of the pump beam at the position of the TEM₀₀-mode is almost negligible. We attribute

this to the multiple emission-reabsorption cycles, the induced thermalization process provides a sufficient photon density for the condensation. Such an effect is unknown in lasers but has already been observed in the context of polariton condensation[32]. As in section 4.2, a complete spatial relaxation of the photon gas is achieved if the pump spot is not moved beyond a distance of $\simeq 50$ μ m from the trap centre. Again this can be attributed to the finite number of emission-reabsorption cycles a photon can undergo before it is lost.

D. Reabsorption cycles

Perhaps the most decisive quantity regarding the degree of thermalization is the average number of reabsorptions of a photon before it is lost from the resonator. The observed spatial redistribution of the photons towards the trap centre already tells us qualitatively that multiple reabsorptions take place in the experiment. A more quantitative measure is experimentally obtainable by a time-resolved measurement, for example of the overall decay time of the microresonator fluorescence. Such a measurement is under current preparation. Nevertheless, already an overall input-output analysis of the data presented in Fig. 13b confirms that the experiments are performed in a regime of multiple reabsorptions, and gives an upper bound for the number of reabsorptions per photon.

From the general conservation of excitations we conclude that the average numbers of excited molecules N_{exc} and the number of photons N_{ph} are linked by

$$N_{\text{exc}} \tau_{\text{exc}}^{-1} \beta = N_{\text{ph}} \tau_{\text{ph}}^{-1}, \quad (23)$$

where τ_{ph} is the average time between emission and reabsorption of a photon, and τ_{exc} the lifetime of the molecular electronic excitation in the resonator. Further, β is the probability that an excited molecule emits into a confined cavity mode rather than decaying radiationless or into an unconfined mode. With this equation we implicitly make the approximation that losses predominantly occur for conversions from molecular excitations to cavity photons but not for the inverse direction, which seems to be justified in our system. N_{exc} is also linked to the absorbed pumping power $P_{\text{p,abs}}$ by

$$\begin{aligned} N_{\text{exc}} &= \frac{P_{\text{p,abs}}}{h\nu_{\text{p}}} \tau_{\text{exc}} (1 + \beta + \beta^2 + \dots) \\ &= \frac{P_{\text{p,abs}}}{h\nu_{\text{p}}} \tau_{\text{exc}} \frac{1}{1 - \beta}, \end{aligned} \quad (24)$$

where $h\nu_{\text{p}}$ is the energy of a pump photon and thus $P_{\text{p,abs}}/h\nu_{\text{p}}$ is the absorbed pump photon rate. The fraction of excitations that were directly created by the pump beam corresponds to the term '1' of the sum, the fraction of excitations that were reabsorbed once corresponds to the term ' β ', and so on. We here assume that the storage time in the resonator is dominated by the lifetime of the

molecular excitation, $\tau_{\text{exc}} \gg \tau_{\text{ph}}$. By the combination of eq. (23) und eq. (24) the probability β can be derived

$$\beta = \frac{1}{1 + \frac{P_{\text{p,abs}} \tau_{\text{ph}}}{h\nu_{\text{p}} N_{\text{ph}}}}, \quad (25)$$

and with that, the average number of reabsorptions per photon $\bar{n}_{\text{re}} = \sum_{n=0}^{\infty} n\beta^n(1-\beta)$ is written as:

$$\bar{n}_{\text{re}} = \frac{h\nu_{\text{p}} N_{\text{ph}}}{P_{\text{p,abs}} \tau_{\text{ph}}}, \quad (26)$$

The lifetime τ_{ph} is experimentally controlled by the dye concentration and is also strongly dependent on the cavity cut-off λ_{c} . For the experimental parameters of Fig. 13a we expect a value of $\tau_{\text{ph}} = (21 \pm 6)$ ps. The absorbed pump power is estimated to be $P_{\text{p,abs}} = (0.65 \pm 0.10)$ mW. With that we obtain $\bar{n}_{\text{re}} = 3.8 \pm 2.5$. The error of this estimate is rather big, nevertheless \bar{n}_{re} is clearly found to be of magnitude 1. The quantitative analysis of the particle flux thus confirms that the experiment is carried out in the regime of multiple scattering. However, it delivers an upper bound of $\bar{n}_{\text{re}} \leq 6$. At first sight this number seems to be relatively small compared to the numerous collisions taking place in an atomic gas. Regarding the degree of thermalization this might seem unfavourable. But one has to consider that, in contrast to atomic collisions, nearly all correlations between absorbed and emitted photon states are annihilated already by a single absorption-emission process (Kasha's rule[63, 81]) - with the only exception of a necessary spatial overlap between both photon states. Thus, the contact with a heat bath, as it takes place in our photon gas experiment, is a much stronger thermalization process compared to two-body collisions in an atomic gas. Experimentally, we have strong evidence for the thermalization to operate both properly in the spatial and the spectral regime, see chapter IV.

E. Selfinteraction of the light condensate

The observed spatial intensity distributions (Fig. 12b) reveal an increase of the condensate diameter with increasing occupation level. The diameter (fwhm) of the transversal ground state as function of N_0/N_{ph} is given explicitly in Fig. 15b. Slightly above criticality the measured diameter of (14 ± 2) μm is in good agreement with the expected ground state diameter of

$$d_0 = 2\sqrt{\hbar \ln 2 / m_{\text{ph}} \Omega}, \quad (27)$$

for non-interacting photons, yielding $d_0 \simeq 14.7$ μm for the parameters of Fig. 12. For higher ground state occupation N_0/N_{ph} this does not hold anymore. This observation suggests the presence of a repelling photon-photon interaction mediated by the dye solution, which can formally be described by a non-zero nonlinear index of refraction, $n_2 \neq 0$, see eq. (8). In our case the dominant

contribution to n_2 seems to be given by a thermo-optical effect. The massively occupied ground state should lead to a small heat gradient in the dye solution due to nonradiative decays. This heat gradient then causes a gradient of the refractive index, which decreases the *optical* distance between the mirrors on the optical axis. Effectively, this can be interpreted as a local distortion of the mirrors, see Fig. 15a, which is indeed expected to lead to a broadening of the ground state mode - in qualitative agreement with the experimental observation.

The index gradient necessary to notably broaden the condensate peak can be estimated by comparing the transversal ground state energy, $\hbar\Omega$, with the interaction term E_{int} of eq. (8)

$$E_{\text{int}} = -\frac{m_{\text{ph}} c^2}{n_0^3} \Delta n, \quad (28)$$

with $\Delta n = n_2 I(\vec{r})$. They become equal for a gradient of $\Delta n \simeq -\hbar\Omega n_0^3 / m_{\text{ph}} c^2$ which in our experiment is roughly $\Delta n \simeq -0.9 \times 10^{-4}$. Such a change in the refractive index is caused by a temperature gradient of $\Delta T = (\partial n / \partial T)^{-1} \Delta n \simeq 0.17$ K, where for methanol we used $\partial n / \partial T \simeq -4.86 \times 10^{-4} \text{ K}^{-1}$ [82], and thus we expect thermal effects to play an important role. In principle, higher orders of polarizability as e.g. the optical Kerr-effect, contribute to the nonlinear index of refraction. This is however expected to be a much weaker process: for an index change of magnitude $\Delta n = 10^{-4}$, an intensity of $I \simeq \Delta n / n_2^{(\text{Kerr})} \simeq 1 \text{ GW/cm}^2$ is necessary, which is 4 to 5 orders of magnitude higher than the intensity building up in the microresonator. Here a nonlinear index of refraction of magnitude $n_2^{(\text{Kerr})} \simeq -1 \times 10^{-13} \text{ cm}^2/\text{W}$ was assumed [83].

The interaction term, eq. (28), can be cast into a more familiar form by introducing the condensate wavefunction $\psi_0(\vec{r})$ via $I(\vec{r}) = (m_{\text{ph}} c^2 / n_0^2 \tau_{\text{rt}}) N_0 |\psi_0(\vec{r})|^2$, where $\tau_{\text{rt}} = \hbar q n_0^2 / m_{\text{ph}} c^2$ is the resonator round trip time. Then eq. (28) reads as

$$E_{\text{int}} = \frac{\hbar^2}{m_{\text{ph}}} \tilde{g} N_0 |\psi_0(\vec{r})|^2, \quad (29)$$

with the dimensionless interaction parameter \tilde{g} given by

$$\tilde{g} = -\frac{m_{\text{ph}}^3 c^4 n_2}{\hbar^2 n_0^5 \tau_{\text{rt}}}. \quad (30)$$

With the interaction term in the form of eq. (29) the similarity of the photon energy given by eq. (8) to the Gross-Pitaevskii (GPE) equation becomes even more apparent. To determine \tilde{g} in our experiment we measure the occupation level N_0/N_{ph} at which the condensate diameter is doubled compared to the non-interacting case, eq. (27). This is achieved roughly at $N_0/N \simeq 0.25$, which corresponds to an occupation number of $N_0 \simeq 40000$. From a numeric solution of the 2d GPE we obtain a doubling of the diameter for an interaction strength of $\tilde{g} N_0 \simeq 30$,

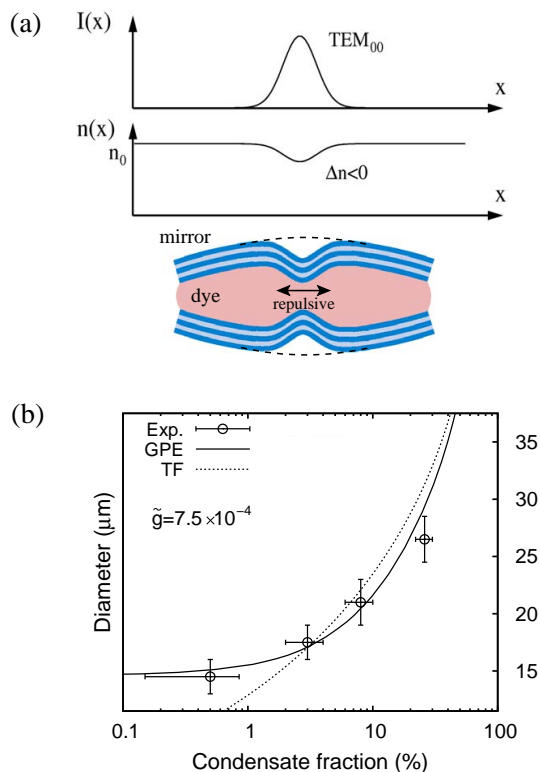


Figure 15: (a) Schematic illustration of the optical self-interaction. The massively occupied ground state is expected to locally heat up the dye solution, reducing the index of refraction and, therefore, shortens the optical distance between the mirrors. This is effectively equivalent to a local deformation of the mirrors (which is shown exaggerated in the figure), resulting in a repulsive interaction. (b) Diameter (fwhm) of the fundamental transversal mode (TEM_{00}) as a function of the condensate fraction (circles). The solid line indicates the theoretically predicted mode diameter for an interaction parameter of $\tilde{g} = 7.5 \times 10^{-4}$ expected from the Gross-Pitaevskii equation, the dashed line gives the diameter expected from a Thomas-Fermi approximation. (experimental parameters as in Fig. 12)

giving the dimensionless interaction parameter in our experiment, $\tilde{g} \simeq 30/40000 = 7(3) \times 10^{-4}$. Fig. 15b shows the experimentally determined data points together with a curve based on the numerical solution to the 2d GPE (solid line) where we used $\tilde{g} = 7.5 \times 10^{-4}$ as an input parameter. Apparently the experimental data can be modelled satisfactorily by this. Additionally, in the figure we have included the condensate diameter (fwhm) according to a Thomas-Fermi approximation (dashed line), given by

$$d_0^{\text{TF}} = 2\sqrt{\hbar/\sqrt{\pi}m_{\text{ph}}\Omega}(\tilde{g}N_0)^{\frac{1}{4}}, \quad (31)$$

which is supposed to yield approximatively correct results for higher condensate fractions, where the transversal kinetic energy of the photons can indeed be neglected.

Compared to the interaction parameters reported for

two-dimensional atomic Bose gases, which are in the regime $\tilde{g} = 10^{-2} - 10^{-1}$ [84], the interactions in the photon gas are at least one order of magnitude smaller. Thus the photon gas is closer to an ideal Bose gas, and there is no indication that the observed phase transition differs from the BEC scenario. This would be expected for stronger interacting gases, where the interactions give rise to a Kosterlitz-Thouless (KT) type of phase [84–86]. An indicator for this would be the loss of long range spatial order. In initial experiments using a shearing interferometer, see Fig. 12, we have tested for the first-order coherence of the condensate by bringing different spatial parts of the condensate to overlap. The observed interference patterns however did not show any signatures of a spatially varying phase. This is in agreement with theoretical expectations, predicting that long range order is lost only for higher values of the dimensionless interaction parameter [84].

VI. CONCLUSIONS

We have investigated thermodynamic properties of a two-dimensional photon gas in a dye-filled optical microcavity. In initial experiments, we have investigated spectral and spatial properties of the photon gas below criticality in detail, and obtained evidence for a thermalized two-dimensional photon gas with non-vanishing chemical potential. When the photon number is increased above a critical value, Bose-Einstein condensation of the photon gas is observed. Experimental signatures are Bose-Einstein distributed transversal excitations including a macroscopic population of the transversal ground mode, the condensation setting in at the expected critical photon number and a spatial relaxation process into the trap centre that can lead to condensation even for a displaced pump spot.

The hitherto performed experiments were focussed on the thermodynamics of the photon gas, a more detailed investigation of the condensate properties is currently performed. Initial interferometric measurements of the condensate peak have already confirmed the first-order coherence of the condensate, with a lower bound for the coherence length of the order of centimeters. We also plan to investigate the second-order coherence [87, 88], which allows to monitor the unusually large particle fluctuations expected from a grand-canonical ensemble. This would allow to further distinguish the radiation emitted by the equilibrium photon BEC from nonequilibrium laser radiation.

On a longer timescale, an experiment based on photonic crystal mirrors with a three-dimensional bandgap [74, 75] should prove advantageous, as losses due to spontaneous emission out of the cavity should be reduced. This would allow to reduce the amount of pumping to maintain the average photon number in the resonator. The full bandgap mirrors together with a condensed matter system, e.g. dye molecules in a polymer matrix, could

even prove useful for technical applications, as it would allow the construction of fluorescence collectors [89], that are more efficient than currently used ones. A tantalizing perspective includes the possible realization of coherent light sources in the UV-regime. Other than in a laser, no inversion is required for the realization of a photon BEC, and spontaneous emission is recaptured [66–68].

On the fundamental research side, we expect the photonic gas within a 'white-wall' box to be a versatile tool. For the ideal Bose gas one does not expect superfluidity, in contrast to the interacting case. Therefore it would be interesting to observe the superfluid properties of the condensate as a function of the dimensionless interaction parameter \tilde{g} . A possible route for the tuning of \tilde{g} would be either the tuning of the photon mass by moving the experiment to the UV spectral region, the reduction of the resonator length by reducing the penetration of the electric field into the mirrors, and by increasing the nonlinear coefficient n_2 . We expect that the interaction parameter of currently $\tilde{g} \approx 7 \times 10^{-4}$ can be increased by at least an order of magnitude, thus allowing to investigate the superfluid properties over a wide range of parameters.

We are aware that the character of the interaction needs to be investigated further. In a different line of experiments, the usage of a second 'heating' dye molecule with low quantum efficiency, whose absorption is spectrally shifted away from the observed spectral region, should allow to thermooptically change the refractive index by means of a heating laser. This would allow the modelling of e.g. periodic lattices, and also more complex potentials for the photon gas, by simply imaging the corresponding pattern onto the 'heating' dye molecules.

Acknowledgments

Financial support from the Deutsche Forschungsgemeinschaft within the focused research unit FOR557 and under contract WE1748/09 is acknowledged.

-
- [1] A. Einstein, Sitzber. Preuss. Akad. Wiss. **1**, 3 (1925)
 - [2] M. H. Anderson, J. R. Ensher, M. R. Matthews, C. E. Wieman, E. A. Cornell, Science **269**, 198 (1995)
 - [3] K. B. Davis, M.-O. Mewes, M. R. Andrews, N. J. van Druten, D. M. Durfee, D. M. Kurn, W. Ketterle, Phys. Rev. Lett. **75**, 3969 (1995)
 - [4] C. C. Bradley, C. A. Sackett, R. G. Hulet, Phys. Rev. Lett. **78**, 985 (1997)
 - [5] S. Jochim, M. Bartenstein, A. Altmeyer, G. Hendl, S. Riedl, C. Chin, J. Hecker, R. Grimm, Science **302**, 2101 (2003)
 - [6] M. Greiner, C. Regal, D. Jin, Nature **426**, 537 (2003)
 - [7] A. J. Leggett, Rev. Mod. Phys. **73**, 307 (2001)
 - [8] A.E. Siegman, *Lasers* (Univ. Science Books, Sausalito, 1986)
 - [9] P.W. Milonni, J.H. Eberly, *Lasers* (Wiley, New York, 1988)
 - [10] M.O. Scully, M.S. Zubairy, *Quantum Optics*, 1st edn. (Cambridge University Press, 1997)
 - [11] M. Planck, Ann. Phys. **309**, 553 (1901)
 - [12] S. Bose, Z. Phys. **26**, 178 (1924)
 - [13] K. Huang, *Statistical Mechanics* (Wiley, New York, 1987)
 - [14] W. Ketterle, D. S. Durfee, D. M. Stamper-Kurn, in *M. Inguscio, S. Stringari und C. E. Wieman (Eds.), Bose-Einstein condensation in atomic gases, Proceedings of the International School of Physics 'Enrico Fermi', Course CXL* (IOS Press, Amsterdam, 1999)
 - [15] Y.B. Zel'dovich, E.V. Levich, Sov. Phys. JETP **28**, 1287 (1969)
 - [16] E. Müller, Physica **139A**, 165 (1986)
 - [17] R. Y. Chiao, Phys. Rev. A **60**, 4114 (1999)
 - [18] R. Y. Chiao, Opt. Commun. **179**, 157 (2000)
 - [19] M. W. Mitchell, C. I. Hancox, R. Y. Chiao, Phys. Rev. A **62**, 043819 (2000)
 - [20] E. L. Bolda, R. Y. Chiao, W. H. Zurek, Phys. Rev. Lett. **86**, 416 (2001)
 - [21] C. F. McCormick, R. Y. Chiao, J. M. Hickmann, Opt. Express **10**, 581 (2002)
 - [22] C. F. McCormick, *Transverse Effects in Nonlinear Optics: Toward the Photon Superfluid* (PhD thesis, University of California, Berkeley, 2003)
 - [23] P. Navez, Phys. Rev. A **68**, 5 (2003)
 - [24] R. Y. Chiao, T. H. Hansson, J. M. Leinaas, S. Viefers, Phys. Rev. A **69**, 063816 (2004)
 - [25] J. Martinez, Anton, J. Opt. Soc. Am. B **23**, 1644 (2006)
 - [26] B. T. Seaman, M. J. Holland, arXiv:0807.1356 (2008)
 - [27] C. Connaughton, C. Josserand, A. Picozzi, Y. Pomeau, S. Rica, Phys. Rev. Lett. **95**, 263901 (2005)
 - [28] C. Conti, M. Leonetti, A. Fratallocchi, L. Angelani, G. Ruocco, Phys. Rev. Lett. **101**, 143901 (2008)
 - [29] P. Aschieri, J. Garnier, C. Michel, V. Doya, A. Picozzi, Phys. Rev. A **83**, 033838 (2011)
 - [30] R. Weill, B. Levit, A. Bekker, B. Fischer, O. Gat, Opt. Express **18**, 16520 (2010)
 - [31] J. Kasprzak et al., Nature **443**, 409 (2006)
 - [32] R. Balili, V. Hartwell, D. Snoke, L. Pfeiffer, Science **316**, 1007 (2007)
 - [33] J. Kasprzak, M. Richard, A. Baas, B. Deveaud, R. André, J.-P. Poizat, L. S. Dang, Phys. Rev. Lett. **100**, 1 (2008)
 - [34] J. Kasprzak, D. D. Solnyshkov, R. André, L. S. Dang, G. Malpuech, Phys. Rev. Lett. **101**, 146404 (2008)
 - [35] K. G. Lagoudakis, M. Wouters, M. Richard, A. Baas, I. Carusotto, R. André, L. S. Dang, B. Deveaud-Plédran, Nature Phys. **4**, 706 (2008)
 - [36] A. Amo, J. Lefrère, S. Pigeon, C. Adrados, C. Ciuti, I. Carusotto, R. Houdré, E. Giacobino, A. Bramati, Nature Phys. **5**, 805 (2009)
 - [37] J. Klaers, F. Vewinger, M. Weitz, Nature Phys. **6**, 512 (2010)
 - [38] J. Klaers, J. Schmitt, F. Vewinger, M. Weitz, Nature

- 468**, 545 (2010)
- [39] E. H. Kennard, Phys. Rev. **11**, 29 (1918)
- [40] E. H. Kennard, Phys. Rev. **29**, 466 (1927)
- [41] B. I. Stepanov, Dokl. Akad. Nauk SSSR+ **112**, 839 (1957)
- [42] L. P. Kazachenko, B. I. Stepanov, Opt. Spektrosk. **2**, 339 (1957)
- [43] J. Klaers, *Bose-Einstein-Kondensation von paraxialem Licht* (PhD thesis, University of Bonn, 2011)
- [44] H. Kogelnik, T. Li, Appl. Optics **5**, 1550 (1966)
- [45] V. Bagnato, D. Kleppner, Phys. Rev. A **44**, 7439 (1991)
- [46] D. S. Petrov, D. M. Gangardt, G. V. Shlyapnikov, J. Phys.-Paris IV **116**, 5 (2004)
- [47] W. J. Mullin, J. Low Temp. Phys. **106**, 615 (1997)
- [48] W. J. Mullin, J. Low Temp. Phys. **110**, 167 (1998)
- [49] H. Yokoyama, S. D. Brorson, J. Appl. Phys. **66**, 4801 (1989)
- [50] E. De Angelis, F. De Martini, P. Mataloni, J. Opt. B-Quantum S. O. **2**, 149 (2000)
- [51] K. H. Drexhage, in *E. Wolf (Ed.), Progress in Optics* (North-Holland, Amsterdam, 1974)
- [52] R. Hulet, E. Hilfer, D. Kleppner, Phys. Rev. Lett. **55**, 2137 (1985)
- [53] W. Jhe, A. Anderson, E. Hinds, D. Meschede, L. Moi, S. Haroche, Phys. Rev. Lett. **58**, 666 (1987)
- [54] F. De Martini, G. Innocenti, G. R. Jacobovitz, P. Mataloni, Phys. Rev. Lett. **59**, 2955 (1987)
- [55] F. De Martini, M. Marrocco, P. Mataloni, L. Crescentini, R. Loudon, Phys. Rev. A **43**, 2480 (1991)
- [56] P. Milonni, J. Mod. Opt. **9**, 119 (2007)
- [57] R. Loudon, M. J. Adams, IET Optoelectron. **1**, 289 (2007)
- [58] D. Meschede, Phys. Rep. **211**, 201 (1992)
- [59] H. Walther, B. T. H. Varcoe, B. G. Englert, T. Becker, Rep. Prog. Phys. **69**, 1325 (2006)
- [60] I. Fujiwara, D. Ter Haar, H. Wergeland, J. Stat. Phys. **2**, 329 (1970)
- [61] R. M. Ziff, G. E. Uhlenbeck, M. Kac, Phys. Rep. **32**, 169 (1977)
- [62] Vi. V. Kocharovskiy, Vl. V. Kocharovskiy, M. Holthaus, C. H. Raymond Ooi, A. A. Svidzinsky, W. Ketterle, M. O. Scully, Adv. Atom. Mol. Opt. Phys. **53**, 291 (2006)
- [63] J. R. Lakowicz, *Principles of fluorescence spectroscopy* (Kluwer Academic, New York, 1999)
- [64] D. A. Sawicki, R. S. Knox, Phys. Rev. A **54**, 4837 (1996)
- [65] J. Klaers, J. Schmitt, T. Damm, F. Vewinger, M. Weitz, in preparation (2011)
- [66] F. De Martini, G. Jacobovitz, Phys. Rev. Lett. **60**, 1711 (1988)
- [67] H. Yokoyama, K. Nishi, T. Anan, Y. Nambu, S. D. Brorson, E. P. Ippen, M. Suzuki, Opt. Quant. Electron. **24**, 245 (1992)
- [68] Y. Yamamoto, S. Machida, G. Björk, Opt. Quant. Electron. **24**, 215 (1992)
- [69] D. Magde, R. Wong, P. G. Seybold, Photochem. Photobiol. **75**, 327 (2002)
- [70] L. R. Wilson, B. S. Richards, Appl. Optics **48**, 212 (2009)
- [71] A. Penzkofer, Y. Lu, Chem. Phys. **103**, 399 (1986)
- [72] A. Penzkofer, W. Leupacher, J. Lumin. **37**, 61 (1987)
- [73] M. Fischer, J. Georges, Chem. Phys. Letters **260**, 115 (1996)
- [74] S. Noda, K. Tomoda, N. Yamamoto, A. Chutinan, Science **289**, 604 (2000)
- [75] A. Blanco et al., Nature **405**, 437 (2000)
- [76] R. Pappalardo, H. Samelson, A. Lempicki, IEEE J. Quantum Elect. **6**, 716 (1970)
- [77] N. Tammuz, R.P. Smith, R.L.D. Campbell, S. Beattie, S. Moulder, J. Dalibard, Z. Hadzibabic, Phys. Rev. Lett. **106**, 230401 (2011)
- [78] F. De Martini, F. Cairo, P. Mataloni, F. Verzegnassi, Phys. Rev. A **46**, 4220 (1992)
- [79] E. Ippen, C. Shank, A. Dienes, IEEE J. Quantum Elect. **7**, 178 (1971)
- [80] O. G. Peterson, S. A. Tuccio, B. B. Snavelly, Appl. Phys. Lett. **17**, 245 (1970)
- [81] M. Kasha, Discuss. Faraday Soc. **9**, 14 (1950)
- [82] M. E. Lusty, M. H. Dunn, Appl. Phys. B-Lasers O. **44**, 193 (1987)
- [83] A. Nag, D. Goswami, J. Photoch. Photobio. A **206**, 188 (2009)
- [84] Z. Hadzibabic, J. Dalibard, in *Proceedings of the International School of Physics "Enrico Fermi", Vol. CLXXIII, "Nano optics and atomics: transport of light and matter waves"* (IOS Press, Amsterdam, 2011)
- [85] Z. Hadzibabic, P. Krüger, M. Cheneau, B. Battelier, J. Dalibard, Nature **441**, 1111 (2006)
- [86] P. Clade, C. Ryu, A. Ramanathan, K. Helmerson, W. D. Phillips, Phys. Rev. Lett. **102**, 170401 (2009)
- [87] R. Hanbury Brown, R.Q. Twiss, Nature **178**, 1046 (1956)
- [88] E.M. Purcell, Nature **178**, 1449 (1956)
- [89] W. van Sark et al., Opt. Express **16**, 21773 (2008)